Efficient 4-Fold Self-Compression of 1.5-mJ Infrared Pulses to 19.8 fs

O. D. Mücke[a]*, S. Ališauskas[a,b], A. J. Verhoef[a], A. Pugžlys[a], V. Smilgevičius[b], J. Pocius[b,c], L. Giniūnas[c], R. Danielius[c], and A. Baltuška[a]
[a]Photonics Institute, Vienna University of Technology, Gusshausstr. 27-387, A-1040 Vienna, Austria
[b]Laser Research Center, Vilnius University, Saulėtekio av. 10, LT-10223 Vilnius, Lithuania
[c]Light Conversion Ltd., P/O Box 1485, Saulėtekio av. 10, LT-10223 Vilnius, Lithuania

ABSTRACT

We demonstrate a four-stage optical parametric chirped-pulse amplification system that delivers carrier-envelope phase-stable ~1.5 μm pulses with energies up to 12.5 mJ before recompression. The system is based on a fusion of femtosecond diode-pumped solid-state Yb technology and a picosecond 100 mJ Nd:YAG pump amplifier. Pulses with 62 nm bandwidth are recompressed to a 74.4 fs duration close to the transform limit. To show the way toward a terawatt-peak-power single-cycle IR source, we demonstrate self-compression of 2.2 mJ pulses down to 19.8 fs duration in a single filament in argon with a 1.5 mJ output energy and 66% energy throughput.

Keywords: optical parametric amplification, filamentation, pulse self-compression, intense few-cycle infrared pulses

1. INTRODUCTION

Optical Parametric Chirped-Pulse Amplification[1] (OPCPA) has attracted a lot of attention as a promising route toward intensity scaling of few-cycle laser pulses. Intense carrier-envelope phase (CEP)-stable few-cycle laser pulses have numerous intriguing applications in attosecond and high-field science[2] including attosecond XUV/soft-X-ray pulse generation[3-5] by high-harmonic generation (HHG), tomographic imaging of molecular orbitals[6], and laser-induced electron diffraction[7]. A major challenge for using HHG in studies of time-resolved tomography of molecular dissociative states is the low ionization potential I_p of excited molecular states. The resulting competition between state depletion and HHG prevents generation of broad HHG spectra necessary for tomographic reconstruction. One solution are laser sources with high ponderomotive energy $U_p \propto \lambda^2 I$ at moderate intensity level, i.e., IR CEP-stable few-cycle high-power laser systems. The present immense interest of the ultrafast community in high-U_p-sources[8-16] has three major reasons:

(1) These sources open the door to previously inaccessible regimes of light-matter interactions[17] and in particular they allow experimental investigations of the λ-scaling laws of strong-field physics[18-21] (Keldysh parameter $\propto\lambda^{-1}$, electron energies $\propto\lambda^2$, HHG cutoff $\propto\lambda^2$, minimum attosecond pulse duration $\propto\lambda^{-1/2}$). In addition, e.g., laser-induced electron diffraction experiments[7] would benefit from IR driving because of the shorter de Broglie electron wavelength and consequently higher spatial resolution.

(2) Because of the λ^2-dependence of the HHG cutoff[22-24], HHG driven by intense few-cycle IR sources holds great promise for the realization of bright coherent sources in the soft- and potentially even hard-X-ray region[25]. The achievable HHG photon fluence depends both on the microscopic single-atom response of the gas and on macroscopic effects in the gas target like phase matching and absorption. At present, both microscopic [$\lambda^{-(5-6)}$-scaling of the single-atom HHG conversion efficiency[18,19,26-28]] and macroscopic parts are subject of a heated scientific debate. Recent work on phase matching of higher harmonics driven by high-energy IR pulses[12,13,25,29-31] indicate the feasibility to compensate the sharp drop of the microscopic HHG efficiency macroscopically by an increased optimal gas pressure for phase matching and a strongly decreasing reabsorption of the generated X-rays at higher photon energies.

(3) The development of high-U_p-sources is also of paramount importance for attosecond photoelectron spectroscopy of solid surfaces[32] and surface-adsorbate systems[33]. Applying the experimental techniques of attosecond science to solid surfaces is very challenging and significantly more difficult than gas-phase experiments because the solid target is not continuously replaced (like in a gas jet), the target density can not be varied (e.g., to reduce space-charge effects), and detection of ions as well as using them as observable is impossible. Nevertheless, Cavalieri *et al.*[32] recently demonstrated

*oliver.muecke@tuwien.ac.at; phone +43 1 58801 38724; fax +43 1 58801 38799; web http://atto.photonik.tuwien.ac.at

International Conference on Ultrafast and Nonlinear Optics 2009, edited by Solomon Saltiel, Alexander Dreischuh, Ivan Christov, Proc. of SPIE Vol. 7501, 750109 · © 2009 SPIE · CCC code: 0277-786X/09/$18 · doi: 10.1117/12.852250

that the attosecond ponderomotive streaking technique can be extended to solid surfaces in a narrow intensity window: space-charge effects originating from above-threshold ionization (ATI) electrons cause a severe background problem if the few-cycle driver pulse intensity is too high. If, on the other hand, the intensity is too low, the ponderomotive streaking is too small to be observed. For a maximum acceptable intensity determined by the experimental conditions (e.g., damage threshold of the solid target, background problems from space-charge effects), IR high-U_p-sources are superior to 0.8-µm Ti:sapphire sources because they exhibit stronger ponderomotive streaking effects.

For many applications in attosecond science, in particular for the generation of isolated attosecond XUV/soft-X-ray pulses[3-5], extremely short pulses comprising only one or two light oscillations underneath the field envelope are required. Ultrabroadband near-degenerate Type-I parametric amplification of CEP-stable two-cycle IR seed pulses obtained from difference-frequency generation (DFG) to the energy level close to 1 mJ has been demonstrated[8-11,16]. However, the inherently low DFG seed energy causes a sizable superfluorescence background[8,9,16] that prevents further energy upscaling. By narrowing the bandwidth of an optical parametric amplifier (OPA), one can optimize the spectral brightness of the seed at the expense of the seed energy, achieve a more uniform saturation across the pulse spectrum, and minimize energy back-conversion into the pump. In saturation, however, the parametrically amplified spectra exhibit steep slopes that lead to poor fidelity of the compressed pulses in the time domain.

The well-established standard technology for the generation of few-cycle driver pulses based on Ti:sapphire amplifier systems is spectral broadening of mJ-level femtosecond pulses in noble gases. Using 5-fs 1-mJ 720-nm driver pulses obtained in this way, coherent X-rays in the keV photon energy range were demonstrated by HHG in He[34]. At present, the energy throughput of gas-phase broadening schemes, such as the hollow-core fiber compressor[35,36] and filamentation[37,38], is limited to 4-5 mJ at 0.8 µm due to ionization losses[39,40]. With our IR pulses we expect to ultimately surpass the present energy limitation for gas broadening schemes[41].

Here, we present a hybrid Type-II IR OPCPA/filamentation approach to pursue a TW-peak-power single-cycle IR source[14,15] that will find many applications in attosecond and high-field science. Our system architecture has several highly attractive features: (1) With the advent of a mature 250 fs Yb:KGW master-oscillator power amplifier (MOPA) it became possible to abandon complex expensive Ti:sapphire front-ends; (2) we avoid working close to the signal-idler wavelength degeneracy and reduce the quantum defect for the signal wave; (3) in OPA stages 2-4, we employ Type-II phase matching in KTP/KTA[42,43] that, as opposed to Type I, supports a much narrower bandwidth but minimizes parasitic self-diffraction[44]; (4) the Yb:KGW master oscillator, centered at 1.04 µm with a FWHM bandwidth of 30 nm, conveniently allows seeding of both the Yb:KGW power amplifier at 1.03 µm and Nd:YAG amplifiers at 1.064 µm for further upscaling of the pulse energy; (5) as discussed below, our scheme automatically results in passive CEP stability.

2. CEP-STABLE MULTIMILLIJOULE INFRARED OPCPA

In this section, we describe in detail a CEP-stable four-stage IR OPCPA system delivering 1.5-µm signal pulses (and corresponding idler pulses at ~3.5 µm) with up to 12.5 mJ pulse energy before recompression. This IR OPCPA is based on a CEP-stable two-stage OPA seed source discussed in subsection 2.1 and two booster-amplification stages presented in subsection 2.2.

2.1 CEP-stable 4-µJ two-stage OPA seed source

The scheme of our two-stage OPA seed source is depicted in Fig. 1.

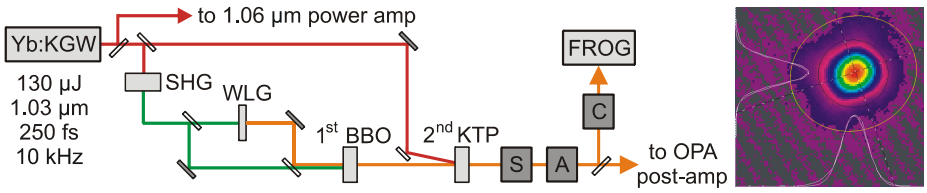

Figure 1. Scheme of the CEP-stable two-stage 1.5-µm OPA seed source. Yb:KGW, 250 fs Yb:KGW MOPA system; SHG, second-harmonic generation in BBO; WLG, white-light generation in sapphire; S/C, grating stretcher/compressor; A, acousto-optic programmable dispersive filter (DAZZLER). Right panel, far-field beam profile of second-stage signal wave.

In our IR OPCPA scheme (see Figs. 1 and 5), both Yb:KGW and Nd:YAG regenerative amplifiers (RAs) are simultaneously seeded from a single master oscillator that has a modest FWHM bandwidth of 30 nm (not shown). To seed the Nd:YAG RA, we pick up unused 1064-nm light behind a transmission grating in the pulse stretcher of the Yb:KGW MOPA. The repetition rate of the Yb:KGW diode-pumped solid state (DPSS) MOPA (Pharos, Light Conversion, Ltd.), tunable in the range of 1-100 kHz, was set at 10 kHz as the 500th harmonic of the flash-lamp-pumped Nd:YAG amplifier (Ekspla Ltd.) operating at 20 Hz. In the Nd:YAG RA, an intracavity etalon is used to narrow the pulse bandwidth and make the pulse duration (60 ps) safe for post amplification.

The 1.03-μm output from the femtosecond Yb:KGW MOPA is first split into two parts by means of a variable beam splitter (consisting of a half-wave plate and a thin-film polarizer); part one is used for implementing the first OPA stage, part two is used for pumping the second OPA stage. In the first OPA stage, the 1.03-μm pulses are first frequency-doubled in a 1-mm thick Type-I BBO crystal (θ=23.4°, φ=90°). Typically 8.5 μJ of 515-nm pulses are again split by a variable beam splitter into two parts: 1.3 μJ (measured behind a variable aperture used for fine-adjusting the input beam diameter) are focused onto a 10-mm thick sapphire plate using an 87-mm focusing lens. In the sapphire plate, a stable white-light (WL) continuum extending to wavelengths >840 nm [see Fig. 2(a)] is created in a single filament. For a sapphire plate thickness of 10 mm we obtain a stronger and more stable WL seed at >780 nm than for thinner plates of 4–6 mm. The WL continuum, which is recollimated with a 40-mm lens, is used to seed the first OPA stage. The WL seed pulses and the 515-nm pump pulses are combined collinearly on a dichroic beam splitter and both are focused onto a 4-mm thick Type-I BBO crystal (θ=22.8°, φ=90°) with an f=20 cm spherical mirror to a $1/e^2$ pump beam diameter of 120 μm. In the pump beam, a variable aperture is used to adjust the pump energy to 1.4 μJ (thus, the parametric gain) and to minimize the detrimental effects of amplified spontaneous emission (ASE). By adjusting both the θ-angle of the BBO crystal and time delay between the seed and pump pulses, different wavelength regions can be phase matched for efficient parametric amplification [Fig. 2(a)]. In particular, selecting the ~795 nm wavelength for amplification, this configuration produces CEP-stable idler pulses[45] at 1.44 μm [Fig. 2(b)] that we use as a seed in the second OPA stage.

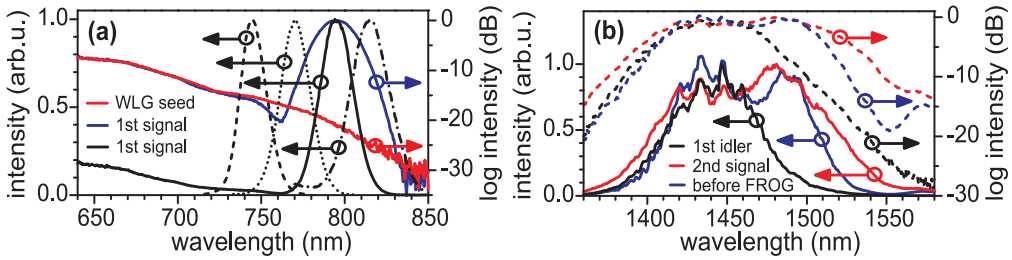

Figure 2. Spectral properties of two-stage 1.5-μm OPA. (a) Near-IR WL seed (red) and signal spectra (blue and black solid) of the first OPA stage. The dashed and dotted curves indicate tunability of the first-stage signal (and corresponding idler). (b) IR CEP-stable seed (black), amplified second-stage signal (red), spectrum before FROG setup (blue). The dashed curves show the same spectra on a logarithmic scale. The amount of ASE is immeasurable in absence of the WL seed.

Following the pioneering work of Kraemer *et al.*[42,43], we employ Type-II KTP/KTA crystals (1.03 μm/1.064 μm pump, ~1.5 μm signal, ~3.3-3.7 μm idler) for the subsequent OPA stages 2-4 because these crystals (unlike borate crystals) are transparent for the mid-IR idler wavelength and exhibit a relatively broad bandwidth around 1.5 μm. The CEP-stable idler pulses from the first OPA stage are recollimated with a 10-cm lens and focused onto a 6-mm thick Type-II KTP crystal (θ=45.5°, φ=0°) using a 50-cm lens. The pump beam is focused onto the same KTP crystal using a 100-cm lens under an (external) walk-off compensation angle of 2.2° with respect to the seed beam. For a pump beam diameter of ~550 μm measured at the KTP crystal input face and 69 μJ (measured behind a variable aperture) pump pulses, we achieve 4 μJ signal pulses, i.e., a pump-signal conversion efficiency of ~6% in the second OPA stage. The pulse-to-pulse intensity fluctuations of the two-stage OPA amounts to 2.5% rms noise, only two times larger than that of the Yb:KGW MOPA pump (1.2% rms). The far-field beam profile of the second-stage signal wave shown in Fig. 1 is nearly Gaussian; the beam propagation factor was determined to be M^2=1.13±0.04 as compared to M^2<1.2 of the Yb:KGW MOPA pump.

The strong nonlinear optical Kerr effect in KTP/KTA [nonlinear refractive index coefficient n_2(KTP/KTA) = 23.7×10^{-16} cm^2/W as compared to n_2(BBO) = 2.9×10^{-16} cm^2/W, from Koechner[46]] raises the important question how severe is pump/idler-to-signal cross-phase modulation (XPM) in the second OPA stage and its effect on CEP stability. The nonlinear effects accumulated during the OPA process in a nonlinear crystal of length L can be quantified by introducing a generalized B-integral

$$B = \frac{2\pi n_2}{\lambda_s}\int_0^L \mathrm{d}z\left[I_s(z) + \gamma_{sp} I_p(z) + \gamma_{si} I_i(z)\right]. \quad (1)$$

The coefficients γ_{sp} and γ_{si}, which quantify the pump-signal and idler-signal coupling, are 2 for parallel polarizations and 2/3 for orthogonal polarizations[47]. For three types of phase matching in the *XZ*-plane[48] (φ=0°) in KTP/KTA OPAs, the values of γ_{sp} and γ_{si}, respectively, are (a) 2/3 and 2 for Type I (e_s+e_i→o_p), (b) 2/3 and 2/3 for Type II (e_s+o_i→o_p), and (c) 2 and 2/3 for Type III (o_s+e_i→o_p). Case (b) as used in our OPA stages 2-4 minimizes the detrimental XPM contribution of pump and idler on the signal wave.

CEP stability of the OPA 2 output was studied by means of inline *f*-to-2*f* interferometry: a supercontinuum is generated by focusing the 1.5-μm pulses into a 3-mm thick sapphire plate with a 15-mm lens. After recollimation, the second harmonic of the 1.5-μm pulses is generated in a 0.2-mm thick Type-I BBO crystal (θ=19.8°, φ=90°). With a polarizer, the supercontinuum and SHG are projected onto a common axis and the resulting *f*-to-2*f* interferograms from 650 to 790 nm are recorded with a spectrometer (see Fig. 3). The observation of stable interference fringes directly proves CEP stability and negligible influence of XPM on the CEP. The slow CEP drift observed in Fig. 3 is clearly of an environmental origin and can easily be compensated for by feedback stabilization of the interferometer formed by the seed and pump paths in the first OPA stage (see Fig. 1).

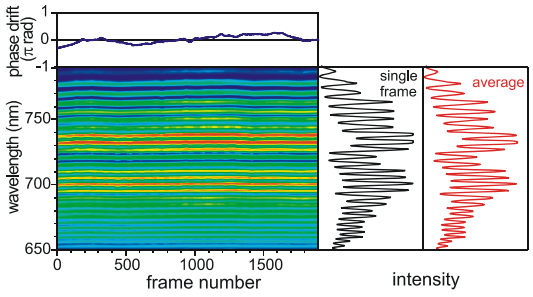

Figure 3. *f*-to-2*f* interferogram exhibiting stable fringes due to CEP stability. The red and black curves in the right panels indicate the spectra averaged over 1900 frames (2 ms frame exposure time) and a single frame, respectively, on the same intensity axis. The blue curve in the above panel indicates the extracted phase drift of the second-stage signal.

In stand-alone applications of our two-stage OPA, the well-behaved spectral phase of the second-stage signal can readily be compensated for by highly reflective chirped mirrors. Here, keeping in mind mainly the development of a >10 mJ four-stage IR OPCPA system, we instead demonstrate that the second-stage output can be stretched to ~40 ps and again recompressed to a sub-40 fs duration using a grating-based stretcher/compressor pair[49] employing 500 grooves/mm 96% efficient gold reflection gratings and an IR high-resolution acousto-optic programmable dispersive filter[50].

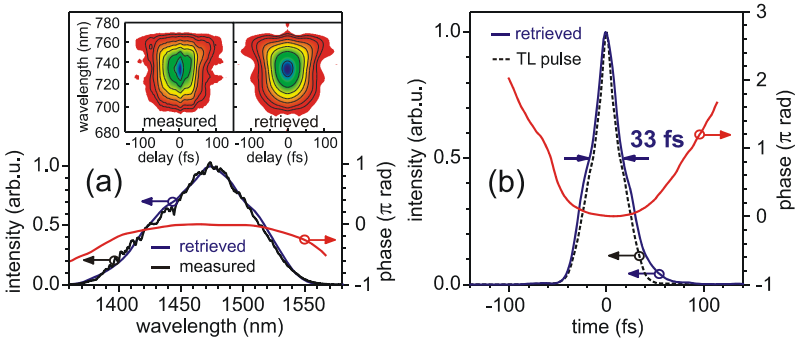

Figure 4. SHG-FROG characterization of the stretched and recompressed 1.47-μm pulses: (a) Measured spectrum (black curve), retrieved spectral intensity (blue) and phase (red). The insets show the measured and retrieved FROG traces. (b) Retrieved temporal intensity (blue) and phase (red) profile indicating a 33-fs FWHM pulse duration. The transform-limited intensity profile (black dashed) corresponds to a 28-fs duration.

Fig. 4 shows SHG-frequency-resolved optical gating (FROG) measurements of 1.47-μm pulses with a 92-nm FWHM bandwidth from the second OPA stage after stretching to ~40 ps and recompression to a 33-fs FWHM pulse duration.

Our two-stage parametric infrared source, easily tunable in the 1.5-1.6 μm range, might find applications in pump-probe experiments on InAs quantum dot semiconductor optical amplifiers operating in the 1.55-μm telecommunications wavelength range[51] or for buried-waveguide writing in semiconductors based on three-photon absorption[52].

2.2 Power-amplification to pulse energies exceeding 10 mJ

In the subsequent booster-amplification stages 3 and 4 shown in Fig. 5, the 1.5-μm signal pulses are amplified from the 4-μJ level to energies >10 mJ before recompression.

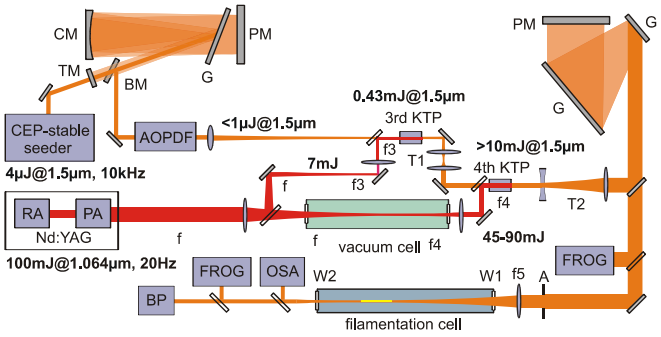

Figure 5. Scheme of the OPCPA power-amplification stages 3 and 4: G, reflection grating; CM, curved mirror; PM, plane mirror; TM/BM, top/bottom mirror; AOPDF, acousto-optic programmable dispersive filter; RA, regenerative amplifier; PA, double-pass post amplifier; f, f3, f4, f5, lens focal lengths; T1, T2, telescopes; A, aperture; W1/W2, input/output windows; BP, beam profiler (pyroelectric 2D array).

As already mentioned in the previous subsection 2.1, in order to optimize the energy extraction from the 60-ps long Nd:YAG pump pulses, the passively CEP-stable 1.5-μm pulses from the front-end are temporally stretched to ~40 ps using a grating-based stretcher. In addition, a high-resolution IR DAZZLER is used for higher-order dispersion control. To guarantee a homogeneous pump profile free of hot spots, we relay-image the 10-mm-diameter crystal rod in the Nd:YAG power amplifier onto the 10-mm thick KTP crystals in stages 3 and 4. The measured surface damage threshold of KTP for our pump pulses (21 GW/cm^2) determines a pump spot diameter of 2 mm and 3.1 mm for stages 3 and 4, respectively. Relay-imaging is achieved with three lenses with focal lengths of f=75 cm, f3=10 cm, and f4=35 cm (see Fig. 5). Because of the larger pump intensities in the fourth OPA stage, the focus needs to be placed inside a vacuum cell to avoid a breakthrough in air. The 1.5-μm (seed) pulses are focused onto the third-stage KTP crystal with a 750-mm lens and imaged onto the fourth-stage KTP crystal with telescope T1. The (external) walk-off compensation angle between pump and seed beam is 2.2°. With this pumping geometry and ~90 mJ pump pulses, we have achieved up to 12.5 mJ signal pulses centered at 1.57 μm with a pump-signal conversion efficiency of ~22% in the final OPCPA stage. To avoid damage to the gold gratings in the OPCPA compressor, we expand the beam diameter of the fourth-stage output by a factor of 5 to 9.5 mm (at the 1/e^2-level) by means of a Galilean beam expander T2.

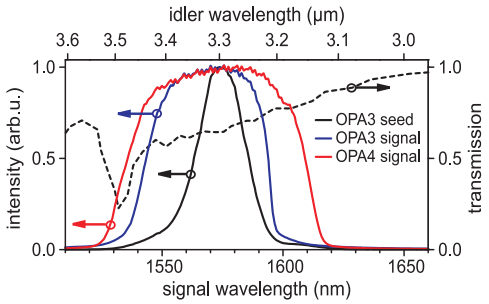

Figure 6. Spectral properties of the power-amplification OPCPA stages: spectrum of the third-stage seed (black curve), amplified signal spectra after stages 3 (blue) and 4 (red). The amount of superfluorescence is immeasurable in absence of the WL seed in OPA stage 1. The dashed curve indicates the idler transmission through 10 mm of KTP.

The spectra of the seed and amplified signal pulses of the power-amplification stages are shown in Fig. 6. In principle, saturating the OPCPA stages permits amplification of pulses with nearly 80 nm bandwidth and ~65-fs Fourier limit. The bandwidth is limited to 80 nm by the 10-mm KTP crystal thickness and operation conditions (seed bandwidth and duration, pump pulse intensity and duration, noncollinearity angle) of the final OPCPA stage. As idler absorption increases above 3.4 μm in KTP, we can achieve higher output powers when tuning the signal center wavelength above 1.55 μm. We also performed experiments using 10-mm thick KTA crystals (θ=46.4°, φ=0°), because idler transmission

only drops slightly to 95% at 3.6 μm. With such KTA crystals we achieved comparable bandwidths (74 nm FWHM), however, against our expectations we have not achieved higher pulse energies.

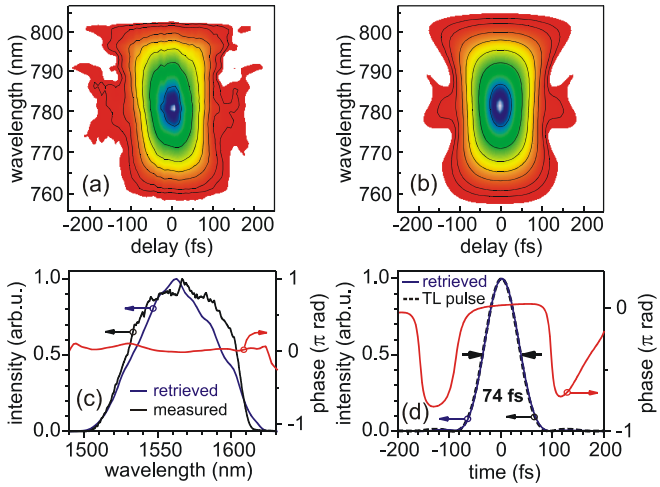

Figure 7. SHG-FROG characterization of the 20-Hz output from the four-stage IR OPCPA: (a) Measured and (b) retrieved FROG traces. (c) Measured spectrum (back curve), retrieved spectral intensity (blue) and phase (red). (d) Retrieved temporal intensity (blue) and phase (red) profiles exhibiting a 74.4-fs FWHM pulse duration. The TL intensity profile (dashed) corresponds to a 72.6-fs duration.

The SHG-FROG data of 3.5-mJ 1.57-μm pulses with 62-nm bandwidth from the 20-Hz four-stage IR OPCPA (see Fig. 7) indicate a 74.4-fs FWHM pulse duration, close to the transform limit (TL) of 72.6 fs. Ultimately, with further optimization sub-70-fs pulse durations seem in reach by recompressing pulses with bandwidths approaching 80 nm.

3. SPECTRAL BROADENING AND PULSE SELF-COMPRESSION VIA FILAMENTATION IN NOBLE GASES

In this section, we demonstrate single-filament IR supercontinuum generation via femtosecond filamentation in noble gases. Depending on the experimental conditions, two filamentation regimes can be achieved: (i) the filamentation regime without plasma-induced pulse self-compression, as discussed in section 3.1, and (ii) the self-compression regime, as discussed in section 3.2. Ultimately, since the critical power of self-focusing scales as λ^2, we expect to surpass the current energy limitation[39,40] (4-5 mJ at 800 nm) with the multi-mJ femtosecond pulses obtained from our IR OPCPA. In addition, a promising route for further pulse energy upscaling is the use of circularly/elliptically polarized input pulses[53,54].

3.1 Multimillijoule filamentation without plasma-induced pulse self-compression

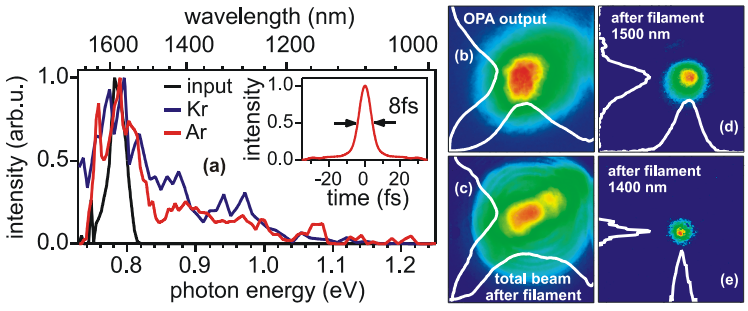

Figure 8. (a) Filamentation of 1.57-μm pulses in noble gases: Individually normalized input (black curve) and output spectra for filamentation of 0.8-mJ pulses in krypton (blue) and 2.5-mJ pulses in argon (red) at a 5 bar pressure. The inset shows the TL intensity profile computed from the argon output spectrum. (b)-(e) Far-field spatial beam profiles measured with the pyroelectric 2D array: (b) before the OPCPA grating compressor; (c) total (frequency-unresolved) beam profile behind the Ar cell; (d) beam profile at 1500 nm; (e) beam profile at 1400 nm. (d) and (e) are taken at the same camera position as (c) by inserting narrowband filters into the beam. Image size is 12.4 mm×12.4 mm.

In our filamentation experiments (see Fig. 5), the 1.57-μm OPCPA pulses were focused using a 50-cm lens placed 4 cm in front of the AR-coated input window W1 of a 138-cm long gas cell filled with argon (I_p=15.76 eV) or krypton (I_p=13.99 eV) at the absolute pressure of 4-5 bar. In the filamentation regime without plasma-induced pulse self-compression (see Fig. 8), we generated ~3-mJ 600-nm-wide IR supercontinua of high spatial quality supporting 8-fs pulse durations, which corresponds to less than two optical cycles at 1.5 μm.

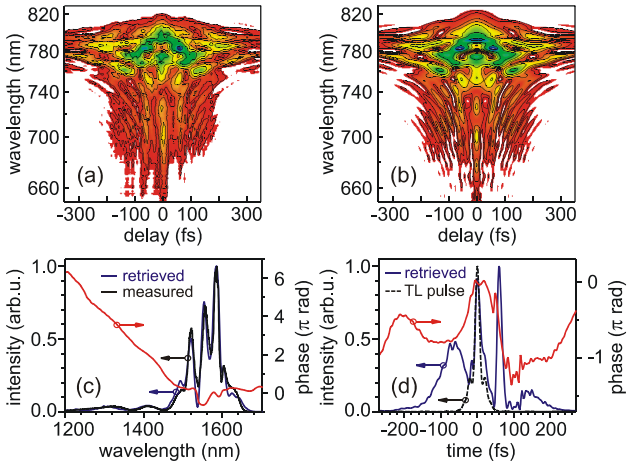

Figure 9. SHG-FROG characterization of 2.1-mJ filamentation output pulses for argon at 4 bar: (a)-(d) as in Fig. 7. The TL intensity profile (dashed) corresponds to a 14.6-fs duration.

SHG-FROG data of such spectrally broadened pulses are displayed in Fig. 9. We emphasize that the FROG characterization (Figs. 9 and 10) and corresponding output pulse energy measurements were performed without aperturing the filamentation output beam. In the experiment shown in Fig. 9, the input pulse energy was 3.0 mJ, output energy 2.1 mJ, corresponding to an energy throughput of 68% including the 8% reflection losses on the uncoated 1-mm thick BK7 output window W2 (see Fig. 5). These SHG-FROG data reveal a rather complex spectro-temporal structure. The observed strong nonlinear phase leads to a temporal break-up into two peaks of 20 fs and 15 fs FWHM duration, separated by 60 fs. Since a clean single-filament spatial profile was observed simultaneously, we conclude that the temporal splitting apparently helps to keep the pulse intensity below the break-up threshold of a single filament.

3.2 Self-compression of millijoule infrared pulses

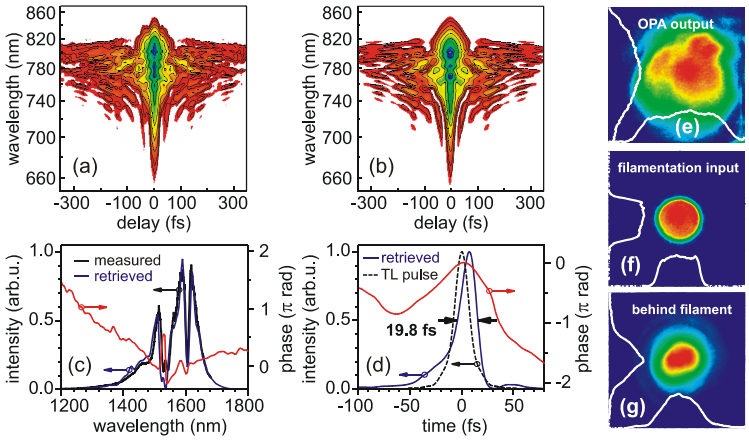

Figure 10. Self-compression of 1.5-mJ pulses in argon at 5 bar: (a)-(d) as in Fig. 7. The retrieved FWHM pulse duration is 19.8 fs, 15.9 fs Fourier limit. (e)-(g) Far-field spatial beam profiles measured with the pyroelectric 2D array: (e) after OPCPA grating compressor; (f) apertured filamentation input behind the iris aperture A; (g) total beam profile behind the filamentation cell. Image size is 12.4 mm×12.4 mm.

The filamentation regime involving plasma-induced pulse self-compression is particularly attractive for the pursuit of TW-peak-power single-cycle IR sources. Recently, Hauri *et al.*[38] demonstrated that filamentation of rather long ~55-fs

OPA pulses at 2 μm in a xenon cell allows the generation of self-compressed 17-fs 0.27-mJ pulses. The limited input pulse energy available in that experiment implied the use of xenon as a noble gas with the highest nonlinearity. Detailed numerical investigation of self-compression of 2-μm laser filaments[41] predicted a number of highly attractive features of femtosecond filamentation at longer carrier wavelength λ: (i) The bandwidth of the generated supercontinuum increases with λ; (ii) for comparable ratios of input power over critical power, P_{in}/P_{crit}, filaments at IR wavelengths have higher pulse energy than near-VIS filaments; (iii) the filament channel extends over longer distances and its waist scales $\propto\lambda$; (iv) self-steepening becomes more pronounced with increasing λ; (v) for gases with moderate ionization potentials (I_p<20 eV, e.g., argon or xenon), the numerical calculations reveal that mid-IR filamentation easily permits self-compression to single-cycle pulse durations, as compared to self-compressed 2-3 cycle durations at visible wavelengths. Self-compression of 2-μm pulses results in supercontinua exhibiting a much flatter spectral phase over the full bandwidth as compared to 800-nm pulses. Bergé[41] also made the important observation that for self-compression of 2-μm pulses, due to nonlinear pulse propagation the shortest achievable pulse duration survives only over shorter distances (~15-20 cm) in the gas medium as compared to the 800-nm case (~60 cm), i.e., the proper choice of the output window position with respect to the filament channel is crucial for observing optimum self-compression.

By lowering the input pulse energy and tuning the gas pressure in the cell, we achieved the regime of pulse self-compression. In the experiment shown in Fig. 10, CEP-stable 2.2-mJ 74.4-fs 1.57-μm input pulses are compressed in a single filament in argon down to a 19.8-fs duration. This represents a temporal compression of the input pulses by a factor of ~4. The output energy was 1.5 mJ, corresponding to the energy throughput of 66%, again including the 8% reflection losses on window W2. The IR supercontinuum with a 130-nm FWHM bandwidth and low-intensity spectral wings extending throughout the VIS originated from a 12-15-cm long filament visible with the naked eye. As argued above, careful optimization of the propagation distance in the pressurized Ar cell behind the filament might lead to the observation of even shorter pulse durations[41]. In addition, the spectral phase is remarkably reproducible on a daily basis which holds potential for further recompression using fixed-dispersion chirped mirrors.

4. CONCLUSIONS

In conclusion, we have demonstrated CEP-stable parametric amplification at 1.5 μm signal wavelength with pulse energies up to 12.5 mJ based on a fusion of a DPSS femtosecond Yb:KGW MOPA system and picosecond Nd:YAG solid-state technology. Moreover, we demonstrated multi-mJ IR supercontinuum generation as well as self-compression of CEP-stable 2.2-mJ 74.4-fs 1.57-μm input pulses down to 19.8 fs duration in a single filament in argon with 1.5 mJ output energy and a 66% energy throughput. The output energy was scaled up by 5.6 times over earlier results[38]. The output energy and energy throughput can be further increased by systematically optimizing the experimental conditions (input pulse energy and beam diameter, focusing lens and position, gas type and pressure, input polarization, gas cell length etc.). Ultimately, with our 1.6-μm pulses we expect to surpass the present energy limitation[39,40] (4-5 mJ at 800 nm) for gas broadening schemes[41].

5. ACKNOWLEDGMENTS

This work has been supported by the Austrian Science Fund (FWF), grants U33-N16 and F1619-N08, LASERLAB-EUROPE II (JRA HAPPIE), and partly supported by the Lithuanian State Science and Studies Foundation (project No. B-42/2009). ODM gratefully acknowledges support from a Lise-Meitner Fellowship by the FWF (project M1094-N14).

REFERENCES

[1] Dubietis, A., Butkus, R. and Piskarskas, A. P., "Trends in Chirped Pulse Optical Parametric Amplification," IEEE J. Sel. Top. Quantum Electron. **12**, 163-172 (2006).
[2] Krausz, F. and Ivanov, M., "Attosecond physics," Rev. Mod. Phys. **81**, 163-234 (2009).
[3] Hentschel, M., Kienberger, R., Spielmann, C., Reider, G. A., Milosevic, N., Brabec, T., Corkum, P., Heinzmann, U., Drescher, M. and Krausz, F., "Attosecond metrology," Nature **414**, 509-513 (2001).
[4] Kienberger, R., Goulielmakis, E., Uiberacker, M., Baltuska, A., Yakovlev, V., Bammer, F., Scrinzi, A., Westerwalbesloh, T., Kleineberg, U., Heinzmann, U., Drescher, M. and Krausz, F., "Atomic transient recorder," Nature **427**, 817-821 (2004).

[5] Sansone, G., Benedetti, E., Calegari, F., Vozzi, C., Avaldi, L., Flammini, R., Poletto, L., Villoresi, P., Altucci, C., Velotta, R., Stagira, S., De Silvestri, S. and Nisoli, M., "Isolated Single-Cycle Attosecond Pulses," Science **314**, 443-446 (2006).
[6] Itatani, J., Levesque, J., Zeidler, D., Niikura, H., Pépin, H., Kieffer, J. C., Corkum, P. B. and Villeneuve, D. M., "Tomographic imaging of molecular orbitals," Nature **432**, 867-871 (2004).
[7] Meckel, M., Comtois, D., Zeidler, D., Staudte, A., Pavičić, D., Bandulet, H. C., Pépin, H., Kieffer, J. C., Dörner, R., Villeneuve, D. M. and Corkum, P. B., "Laser-Induced Electron Tunneling and Diffraction," Science **320**, 1478-1482 (2008).
[8] Fuji, T., Ishii, N., Teisset, C. Y., Gu, X., Metzger, T., Baltuška, A., Forget, N., Kaplan, D., Galvanauskas, A. and Krausz, F., "Parametric amplification of few-cycle carrier-envelope phase-stable pulses at 2.1 μm," Opt. Lett. **31**, 1103-1105 (2006).
[9] Gu, X., Marcus, G., Deng, Y., Metzger, T., Teisset, C., Ishii, N., Fuji, T., Baltuska, A., Butkus, R., Pervak, V., Ishizuki, H., Taira, T., Kobayashi, T., Kienberger, R. and Krausz, F., "Generation of carrier-envelope-phase-stable 2-cycle 740-μJ pulses at 2.1-μm carrier wavelength," Opt. Express **17**, 62-69 (2009).
[10] Vozzi, C., Cirmi, G., Manzoni, C., Benedetti, E., Calegari, F., Sansone, G., Stagira, S., Svelto, O., De Silvestri, S., Nisoli, M. and Cerullo, G., "High-energy, few-optical-cycle pulses at 1.5 μm with passive carrier-envelope phase stabilization," Opt. Express **14**, 10109-10116 (2006).
[11] Vozzi, C., Calegari, F., Benedetti, E., Gasilov, S., Sansone, G., Cerullo, G., Nisoli, M., De Silvestri, S. and Stagira, S., "Millijoule-level phase-stabilized few-optical-cycle infrared parametric source," Opt. Lett. **32**, 2957-2959 (2007).
[12] Takahashi, E. J., Kanai, T., Nabekawa, Y. and Midorikawa, K., "10 mJ class femtosecond optical parametric amplifier for generating soft x-ray harmonics," Appl. Phys. Lett. **93**, 041111-1-3 (2008).
[13] Takahashi, E. J., Kanai, T., Ishikawa, K. L., Nabekawa, Y. and Midorikawa, K., "Coherent Water Window X Ray by Phase-Matched High-Order Harmonic Generation in Neutral Media," Phys. Rev. Lett. **101**, 253901-1-4 (2008).
[14] Mücke, O. D., Sidorov, D., Dombi, P., Pugžlys, A., Baltuška, A., Ališauskas, S., Smilgevičius, V., Pocius, J., Giniūnas, L., Danielius, R. and Forget, N., "Scalable Yb-MOPA-driven carrier-envelope phase-stable few-cycle parametric amplifier at 1.5 μm," Opt. Lett. **34**, 118-120 (2009).
[15] Mücke, O. D., Ališauskas, S., Verhoef, A. J., Pugžlys, A., Baltuška, A., Smilgevičius, V., Pocius, J., Giniūnas, L., Danielius, R. and Forget, N., "Self-compression of millijoule 1.5 μm pulses," Opt. Lett. **34**, 2498-2500 (2009).
[16] Moses, J., Huang, S.-W., Hong, K.-H., Mücke, O. D., Falcão-Filho, E. L., Benedick, A., Ilday, F. Ö., Dergachev, A., Bolger, J. A., Eggleton, B. J. and Kärtner, F. X., "Highly stable ultrabroadband mid-IR optical parametric chirped-pulse amplifier optimized for superfluorescence suppression," Opt. Lett. **34**, 1639-1641 (2009).
[17] Blaga, C. I., Catoire, F., Colosimo, P., Paulus, G. G., Muller, H. G., Agostini, P. and DiMauro, L. F., "Strong-field photoionization revisited," Nature Phys. **5**, 335-338 (2009).
[18] Tate, J., Auguste, T., Muller, H. G., Salières, P., Agostini, P. and DiMauro, L. F., "Scaling of Wave-Packet Dynamics in an Intense Midinfrared Field," Phys. Rev. Lett. **98**, 013901-1-4 (2007).
[19] Colosimo, P., Doumy, G., Blaga, C. I., Wheeler, J., Hauri, C., Catoire, F., Tate, J., Chirla, R., March, A. M., Paulus, G. G., Muller, H. G., Agostini, P. and DiMauro, L. F., "Scaling strong-field interactions towards the classical limit," Nature Phys. **4**, 386-389 (2008).
[20] Doumy, G., Wheeler, J., Roedig, C., Chirla, R., Agostini, P. and DiMauro, L. F., "Attosecond Synchronization of High-Order Harmonics from Midinfrared Drivers," Phys. Rev. Lett. **102**, 093002-1-4 (2009).
[21] Agostini, P. and DiMauro, L. F., "Atoms in high intensity mid-infrared pulses," Contemp. Phys. **49**, 179–197 (2008).
[22] Sheehy, B., Martin, J. D. D., DiMauro, L. F., Agostini, P., Schafer, K. J., Gaarde, M. B. and Kulander, K. C., "High Harmonic Generation at Long Wavelengths," Phys. Rev. Lett. **83**, 5270-5273 (1999).
[23] Shan, B. and Chang, Z., "Dramatic extension of the high-order harmonic cutoff by using a long-wavelength driving field," Phys. Rev. A **65**, 011804(R)-1-4 (2001).
[24] Gordon, A. and Kärtner, F. X., "Scaling of keV HHG photon yield with drive wavelength," Opt. Express **13**, 2941-2947 (2005).
[25] Popmintchev, T., Chen, M.-C., Bahabad, A., Gerrity, M., Sidorenko, P., Cohen, O., Christov, I. P., Murnane, M. M. and Kapteyn, H. C., "Phase matching of high harmonic generation in the soft and hard X-ray regions of the spectrum," Proc. Natl. Acad. Sci. USA **106**, 10516-10521 (2009).
[26] Schiessl, K., Ishikawa, K. L., Persson, E. and Burgdörfer, J., "Quantum Path Interference in the Wavelength Dependence of High-Harmonic Generation," Phys. Rev. Lett. **99**, 253903-1-4 (2007).

[27] Shiner, A. D., Trallero-Herrero, C., Kajumba, N., Bandulet, H.-C., Comtois, D., Légaré, F., Giguère, M., Kieffer, J.-C., Corkum, P. B. and Villeneuve, D. M., "Wavelength Scaling of High Harmonic Generation Efficiency," Phys. Rev. Lett. **103**, 073902-1-4 (2009).
[28] Frolov, M. V., Manakov, N. L., Sarantseva, T. S., Emelin, M. Y., Ryabikin, M. Y. and Starace, A. F., "Analytic Description of the High-Energy Plateau in Harmonic Generation by Atoms: Can the Harmonic Power Increase with Increasing Laser Wavelengths?," Phys. Rev. Lett. **102**, 243901-1-4 (2009).
[29] Popmintchev, T., Chen, M.-C., Cohen, O., Grisham, M. E., Rocca, J. J., Murnane, M. M. and Kapteyn, H. C., "Extended phase matching of high harmonics driven by mid-infrared light," Opt. Lett. **33**, 2128-2130 (2008).
[30] Yakovlev, V. S., Ivanov, M. and Krausz, F., "Enhanced phase-matching for generation of soft X-ray harmonics and attosecond pulses in atomic gases," Opt. Express **15**, 15351-15364 (2007).
[31] Falcão-Filho, E. L., Gkortsas, V. M., Gordon, A. and Kärtner, F. X., "Analytic scaling analysis of high harmonic generation conversion efficiency," Opt. Express **17**, 11217-11229 (2009).
[32] Cavalieri, A. L., Müller, N., Uphues, T., Yakovlev, V. S., Baltuška, A., Horvath, B., Schmidt, B., Blümel, L., Holzwarth, R., Hendel, S., Drescher, M., Kleineberg, U., Echenique, P. M., Kienberger, R., Krausz, F. and Heinzmann, U., "Attosecond spectroscopy in condensed matter," Nature **449**, 1029-1032 (2007).
[33] Miaja-Avila, L., Saathoff, G., Mathias, S., Yin, J., La-o-vorakiat, C., Bauer, M., Aeschlimann, M., Murnane, M. M. and Kapteyn, H. C., "Direct Measurement of Core-Level Relaxation Dynamics on a Surface-Adsorbate System," Phys. Rev. Lett. **101**, 046101-1-4 (2008).
[34] Seres, J., Seres, E., Verhoef, A. J., Tempea, G., Streli, C., Wobrauschek, P., Yakovlev, V., Scrinzi, A., Spielmann, C. and Krausz, F., "Source of coherent kiloelectronvolt X-rays," Nature **433**, 596 (2005).
[35] Nisoli, M., De Silvestri, S. and Svelto, O., "Generation of high energy 10 fs pulses by a new pulse compression technique," Appl. Phys. Lett. **68**, 2793-2795 (1996).
[36] Nisoli, M., De Silvestri, S., Svelto, O., Szipöcs, R., Ferencz, K., Spielmann, C., Sartania, S. and Krausz, F., "Compression of high-energy laser pulses below 5 fs," Opt. Lett. **22**, 522-524 (1997).
[37] Hauri, C. P., Kornelis, W., Helbing, F. W., Heinrich, A., Couairon, A., Mysyrowicz, A., Biegert, J. and Keller, U., "Generation of intense, carrier-envelope phase-locked few-cycle laser pulses through filamentation," Appl. Phys. B **79**, 673-677 (2004).
[38] Hauri, C. P., Lopez-Martens, R. B., Blaga, C. I., Schultz, K. D., Cryan, J., Chirla, R., Colosimo, P., Doumy, G., March, A. M., Roedig, C., Sistrunk, E., Tate, J., Wheeler, J., DiMauro, L. F. and Power, E. P., "Intense self-compressed, self-phase-stabilized few-cycle pulses at 2 μm from an optical filament," Opt. Lett. **32**, 868-870 (2007).
[39] Suda, A., Hatayama, M., Nagasaka, K. and Midorikawa, K., "Generation of sub-10-fs, 5-mJ-optical pulses using a hollow fiber with a pressure gradient," Appl. Phys. Lett. **86**, 111116-1-3 (2005).
[40] Stibenz, G., Zhavoronkov, N. and Steinmeyer, G., "Self-compression of millijoule pulses to 7.8 fs duration in a white-light filament," Opt. Lett. **31**, 274-276 (2006).
[41] Bergé, L., "Self-compression of 2 μm laser filaments," Opt. Express **16**, 21529-21543 (2008).
[42] Kraemer, D., Hua, R., Cowan, M. L., Franjic, K. and Miller, R. J. D., "Ultrafast noncollinear optical parametric chirped pulse amplification in $KTiOAsO_4$," Opt. Lett. **31**, 981-983 (2006).
[43] Kraemer, D., Cowan, M. L., Hua, R., Franjic, K. and Miller, R. J. D., "High-power femtosecond infrared laser source based on noncollinear optical parametric chirped pulse amplification," J. Opt. Soc. Am. B **24**, 813-818 (2007).
[44] Varanavičius, A., Dubietis, A., Beržanskis, A., Danielius, R. and Piskarskas, A., "Near-degenerate cascaded four-wave mixing in an optical parametric amplifier," Opt. Lett. **22**, 1603-1605 (1997).
[45] Baltuška, A., Fuji, T. and Kobayashi, T., "Controlling the Carrier-Envelope Phase of Ultrashort Light Pulses with Optical Parametric Amplifiers," Phys. Rev. Lett. **88**, 133901-1-4 (2002).
[46] Koechner, W, [Solid-State Laser Engineering], 6th edition, Springer, Berlin (2006).
[47] Agrawal, G. P., [Nonlinear Fiber Optics], 4th edition, Academic Press, New York (2007).
[48] Liu, H. J., Chen, G. F., Zhao, W., Wang, Y. S., Wang, T. and Zhao, S. H., "Phase matching analysis of noncollinear optical parametric process in nonlinear anisotropic crystals," Opt. Commun. **197**, 507-514 (2001).
[49] Kalashnikov, M. P., Risse, E., Schönnagel, H. and Sandner, W., "Double chirped-pulse-amplification laser: a way to clean pulses temporally," Opt. Lett. **30**, 923-925 (2005).
[50] Verluise, F., Laude, V., Huignard, J.-P., Tournois, P. and Migus, A., "Arbitrary dispersion control of ultrashort optical pulses with acoustic waves," J. Opt. Soc. Am. B **17**, 138-145 (2000).
[51] Zilkie, A. J., Meier, J., Smith, P. W. E., Mojahedi, M., Aitchison, J. S., Poole, P. J., Allen, C. N., Barrios, P. and Poitras, D., "Femtosecond gain and index dynamics in an InAs/InGaAsP quantum dot amplifier operating at 1.55 μm," Opt. Express **14**, 11453-11459 (2006).

[52] Nejadmalayeri, A. H., Herman, P. R., Burghoff, J., Will, M., Nolte, S. and Tünnermann, A., "Inscription of optical waveguides in crystalline silicon by mid-infrared femtosecond laser pulses," Opt. Lett. **30**, 964-966 (2005).
[53] Trisorio, A. and Hauri, C. P., "Control and characterization of multiple circularly polarized femtosecond filaments in argon," Opt. Lett. **32**, 1650-1652 (2007).
[54] Varela, O., Zaïr, A., San Román, J., Alonso, B., Sola, I. J., Prieto, C. and Roso, L., "Above-millijoule super-continuum generation using polarisation dependent filamentation in atoms and molecules," Opt. Express **17**, 3630-3639 (2009).